AIAA JOURNAL
Vol. 39, No. 12, December 2001

Active-Control System for Breakup of Airplane Trailing Vortices

J. D. Crouch,* G. D. Miller,† and P. R. Spalart‡
The Boeing Company, Seattle, Washington 98124-2207

Wing control surfaces are used to trigger the breakup of trailing vortices behind aircraft in a flaps-down configuration. In the near field of the aircraft there are multiple pairs of vortices, which admit new instability mechanisms that do not exist on a single pair of vortices. A periodic motion of the control surfaces is used to introduce a unique form of perturbation that is amplified in the multiple vortex-pair system but conserves total circulation, lift, and rolling moment. Growth of the perturbations leads to the periodic pinching of the starboard and port vortices into a series of vortex rings. The concept is demonstrated using numerical simulations and towing-tank experiments. Results show that the system breaks up the trailing vortices more rapidly than a comparable excitation of the Crow instability on a single pair of vortices. The overall effectiveness of the system depends on the airplane configuration, namely, details of the flap system and the horizontal tail.

Nomenclature

$\tilde{b}_w$	=	wing vorticity centroid spacing
C_L	=	total wing/body lift coefficient
f	=	nondimensional forcing frequency, V_A/λ
V_A	=	nondimensional airplane speed
α	=	nondimensional wave number, $2\pi/\lambda$
Γ_f	=	nondimensional flap-vortex circulation, $\tilde{\Gamma}_f/\tilde{\Gamma}_w$
Γ_T	=	nondimensional tip-vortex circulation, $\tilde{\Gamma}_T/\tilde{\Gamma}_w$
Γ_t	=	nondimensional tail-vortex circulation, $\tilde{\Gamma}_t/\tilde{\Gamma}_w$
$\tilde{\Gamma}_w$	=	wing circulation
$\Delta C_L/C_L$	=	level of lift shifted during forcing cycle
Δy_T	=	nondimensional peak-to-peak tip-vortex y perturbation
Δz_T	=	nondimensional peak-to-peak tip-vortex z perturbation
δ	=	flap- and tip-vortex spacing parameter, $[(y_T - y_f)^2 + (z_T - z_f)^2]^{1/2}$
λ	=	nondimensional instability wavelength
τ	=	nondimensional time, $\tilde{t}/(2\pi\tilde{b}_w^2/\tilde{\Gamma}_w)$

Subscripts

ell	=	values based on elliptic spanload approximation
f	=	inboard-flap vortex
T	=	tip vortex
t	=	horizontal-tail vortex
w	=	wing vorticity, sum of tip and flap vortices
0	=	total half-plane vorticity

I. Introduction

A. Background

TRAILING vortices in the wakes of aircraft are an unavoidable byproduct of finite span lifting wings. Airplanes create trailing vortices (rotation of the air), due to the pressure differences that produce the lift of the wing. The rotation and the associated downflow (between the vortices) and upflow (outside the vortices) can severely disrupt the flight of a following aircraft that enters the wake of a leading aircraft, creating a potential safety hazard. In general, the trailing vortices are transported away from the flight path by the self-induction of the rotating flow and by atmospheric currents. However, there are instances when atmospheric effects counter the self-induction of the vortices, potentially creating a hazardous condition for following aircraft on the same flight path. Aircraft can also intercept the glide path of another aircraft from below, placing their trajectory on a wake that has descended normally from the proceeding aircraft's flight path. Several accidents have been attributed to wake turbulence over the past 15 years, the majority of which occurred on approach and landing under visual flight rules. Flight operations under instrument flight rules must satisfy specific, and more stringent, wake-vortex spacing requirements for airplanes that are in approach to landing at the same airport.

Because of the spacing requirements for airplanes on approach, trailing vortices play a role in determining the capacity of commercial airports. Because the wake-turbulence spacing is often larger than the spacing required by other factors such as radar resolution or runway occupancy, under some conditions it adds to the congestion and delays in the air transportation system. For example, Robinson[1] estimated that the current Federal Aviation Administration (FAA) wake-turbulence separations result in a 12% loss in capacity when arrivals comprise 50% of the operations. This estimate is based on simulations for 10 major U.S. airports with the assumption that the separations would be based on radar procedures in the absence of wake-vortex constraints.

The safety hazards associated with trailing-vortex upsets and the impact of vortex separations on airport capacity have motivated numerous studies aimed at wake-vortex upset prevention. The most effective means of upset prevention would be to remove the threat by alleviating or destroying the vortices. Short of this, the next best solution would be to enable the following aircraft to tolerate the vortex encounter. If the vortex threat cannot be removed, or tolerated, then it must be avoided.

The current work aims at wake-vortex upset prevention by seeking to reduce the vortex threat using an active-control system on the lead aircraft. Prior attempts at wake-vortex alleviation can be grouped into two categories: methods to modify the vortex structure, for example, core size, and methods to break up the vortices by exploiting natural instabilities.[2] Methods that modify the vortex structure can reduce the peak velocities in the vortices but not the total vortex circulation, primarily benefiting following aircraft that are much smaller than the lead aircraft. The active system considered here seeks to force the breakup of the vortices.

B. Previous Efforts Toward Vortex Breakup

A method for enhancing the breakup of the vortices was first suggested by Crow[3] and later presented by Crow and Bate.[4] Airplane control surfaces were to be used to oscillate the wing loading inboard and outboard in a prescribed fashion to excite the Crow instability.[5] The Crow instability is a sinuous mode that exists on a single pair of counter-rotating vortices. The growth of the instability

Received 22 July 2000; revision received 25 February 2001; accepted for publication 14 May 2001.

*Associate Technical Fellow, Enabling Technology and Research, Boeing Commercial Airplanes.
†Principal Engineer, Enabling Technology and Research, Boeing Commercial Airplanes.
‡Technical Fellow, Enabling Technology and Research, Boeing Commercial Airplanes.

leads to periodic (in the flight-path direction) linking of the vortices from the starboard and port sides. The linking transforms the vortices into vortex rings, which, after some additional time, become significantly deformed (or break up). This linking can be observed quite frequently in natural conditions, when atmospheric turbulence seeds the instability.

The concept of exciting the Crow instability[5] was tested in towing-tank experiments of Bilanin and Widnall.[6] The experiments showed that the instability could, in fact, be excited by periodically shifting the wing lift. However, to break up the vortices through excitation of the Crow instability[5] (within a useful time span), significant movement of the vorticity centroids is required. Also, to preserve total lift while moving the vorticity centroids, the wing-root loading must vary in proportion to the vortex perturbation. As a result, significant movement in the wing lift is required for excitation of the Crow instability. The large shifts in the wing lift result in excessive loss in the baseline wing lift and undesirably large unsteady forces on the airplane. The baseline lift is reduced with active control because part of the wing lift, either inboard or outboard, is being forfeited at any time during the forcing cycle.

The analysis of Crow[5] considered a single pair of trailing vortices, as observed far downstream of an aircraft. In the near field of a flaps-down configuration, there are multiple trailing-vortex pairs.[7] This near-field system of vortices admits new instability and transient-growth mechanisms.[8,9] These growth mechanisms, like the Crow instability,[5] involve waveforms that are fixed with respect to the ground; that is, zero frequency in the ground-based reference frame. Thus, they are unsteady in the airplane reference frame.

There has been some effort focused on the possible benefits of exciting the multiple-vortex system to enhance the breakup of the vortices. Rossow[10] considered a system of multiple vortex pairs to help explain flight-test results that showed vortex attenuation behind a 747 during roll oscillations (see Barber and Tymczyszyn[11] for flight-test details). Rossow[10] considered a pair of wing-tip vortices, a pair of vortices from the outboard edge of the inboard flap, and a pair of vortices of opposite rotation from the inboard edge of the inboard flap, or side of body. This system of vortices showed a significant amplification to antisymmetric roll-induced perturbations, but no amplification improvement beyond the Crow instability[5] for symmetric pitch-induced perturbations. Rennich and Lele[12] proposed a breakup scheme based on a special configuration of two trailing-vortex pairs. They considered an outboard pair resulting from the drop in lift at the wing tip and an inboard pair, of opposite rotation, resulting from the drop in lift at the airplane side of body. When the strengths and positions of the vortices were chosen to keep the vortices nearly in-plane as they propagate downward, significant amplification was observed. This produced a more efficient forcing scheme compared to that of Crow,[3] but Rennich and Lele's scheme[12] is limited to specific (and hard to control) ratios of vortex strength and spacing. Also, in practice, the vortices produced at the side of body are short lived due to the high level of turbulent mixing in the body wake and their close proximity to one another.

We consider an alternative approach that exploits the multiple-vortex growth mechanisms analyzed by Crouch[9] as extended to a more complete model of the near-field vortex system. Similar to the earlier efforts, airplane control surfaces are used to introduce vortex perturbations. However, the magnitude and form of the perturbations differ significantly from the earlier work.

II. Problem Formulation for Flaps-Down Configurations

A. Basic System of Airplane Trailing Vortices

We consider the vortex system created by an airplane on approach with flaps down. The flaps-down configuration produces multiple trailing vortices from the wing that remain distinct for some distance behind the aircraft. In addition to the wing vortices (which, in the simplest case, can be modeled as a pair of corotating vortices on each side of the aircraft) there are tail vortices that rotate counter to the wing vortices. Figure 1 shows the essential vortex system in the near field of the flaps-down configuration. We introduce a Cartesian coordinate system with x along the flight path, y in the span direction, and z in the vertical direction.

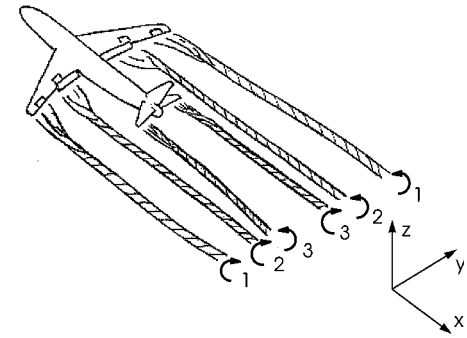

Fig. 1 Schematic of flaps-down aircraft showing 1, tip vortices; 2, inboard-flap vortices; and 3, horizontal-tail vortices.

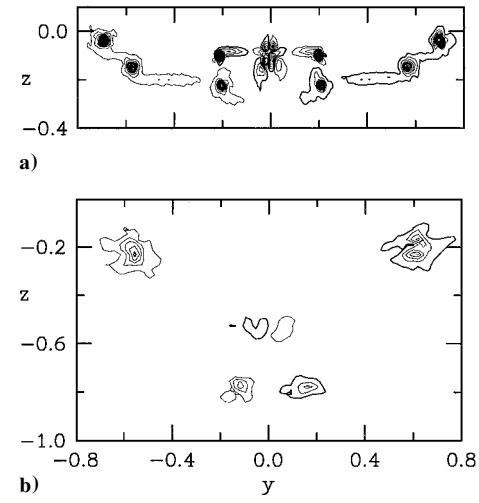

Fig. 2 Vorticity surveys behind an aircraft with flaps down measured at a) tail plane $\tau = 0$ and b) downstream at $\tau = 0.2$, showing wing-tip vortices, outboard-flap vortices, inboard-flap vortices, and horizontal-tail vortices.

The near-field dynamics of the multiple-vortex system depends on the circulations and positions (Γ, y, and z) of the different vortices. The subscripts T, f, and t are introduced for the tip, flap, and tail vortices, respectively. Quantities are nondimensionalized using the wing circulation $\tilde{\Gamma}_w = \tilde{\Gamma}_T + \tilde{\Gamma}_f$ and wing-vorticity centroid spacing $\tilde{b}_w$, where the tilde represents a dimensional quantity. This introduces the nondimensional timescale $\tau = \tilde{t}/(2\pi \tilde{b}_w^2/\tilde{\Gamma}_w)$. The distance behind the aircraft Δx is related to τ by $\Delta x = \tau V_A$, where V_A is the nondimensional airplane velocity. Essential features of the wing spanload (i.e., the distribution of lift along the wing) can be modeled by two nondimensional parameters: the flap-vortex circulation Γ_f and the vortex separation distance $\delta = [(y_T - y_f)^2 + (z_T - z_f)^2]^{1/2}$. The use of a single measure δ for the position of the flap vortex is motivated by the two-pair model[9] and is found to be adequate for the more general system. The tail vortices are described by the three nondimensional parameters Γ_t, y_t, and z_t, where z_t is referenced to the centroid of wing vorticity. Here these parameters are based on measurements at the tail of the airplane.

Wind-tunnel wake surveys show that the trailing-edge vortex sheet has evolved into compact vortices within about one span of distance downstream of the aircraft. Figure 2 shows the vorticity distribution behind the current test model, which mimics a commercial aircraft with landing flaps. The measurements are just downstream of the tail at $\tau \equiv 0$ and approximately four spans farther downstream at $\tau = 0.2$. These wake surveys were made using the five-hole probe and two rotary-axis traverser system and the data analysis technique described by Crowder et al.[13] The dominant features of the wake behind the test model are similar to wakes behind wind-tunnel models of commercial airplanes (see Sec. IV for additional experimental details).

At $\tau = 0$, the vorticity is concentrated into nearly discrete vortices associated with the wing tip, the outer edge of the outer flap,

the outer edge of the inner flap, the horizontal tail, and the side of body. For this spanload, there are no distinct vortices from the inner edge of the outer flap. The contour levels are the same for Figs. 2a and 2b; the minimum contour is about 2.5% of the peak vorticity value in Fig. 2a. The side of body vortices are close together and in the wake of the airplane body, and so they do not persist very far downstream. The vortices from the outer edge of the outer flap and the wing tip merge to form a single pair of tip vortices. The resulting vortex system consist of the tip vortices, the inboard-flap vortices, and the tail vortices similar to the schematic of Fig. 1. Although the downstream measurement station (for example, Fig. 2b) provides a better indication of the strengths and persistence of the different vortices, in general, information this far downstream is not available from wind-tunnel tests and cannot be inferred from the spanload with current methods. Also, the choice of the downstream location is arbitrary, and the results generally depend on the location. Thus, the reference parameters used to characterize the different configurations will be measured just downstream of the tail. From Fig. 2a, the key parameters are $\Gamma_f = 0.26$, $\delta = 0.42$, $\Gamma_t = -0.22$, $y_t = 0.19$, and $z_t - z_w = 0.04$.

By the downstream location ($\tau = 0.2$), the inboard vortices and the tail vortices have propagated toward the centerline. The tail vortices are positioned above the flap vortices in Fig. 2b. Sufficiently far downstream, the distinct vortices on each side of the aircraft typically give way to a single vortex pair. This can result from vortex merger, vortex cancellation (on the centerline), and/or vortex escape, that is, from the influence of the stronger tip vortices. Towing-tank experiments show that the typical scenario (for the parameters considered here) is for the tail vortices to be partially or completely canceled by colliding on the centerline. The flap vortices then continue to orbit the tip vortices. In this case, the primary effect of the tail vortices is to enlarge the vortex separation distance δ by forcing the flap vortices closer to the centerline.

B. Growth Mechanisms for Multiple Vortex Pairs

This system of vortices (tip and flap, or tip, flap, and tail) admits new growth mechanisms that lead to rapid distortion of the vortices when proper initial perturbations are imposed.[8,9] Three potential growth mechanisms have been identified for a two-vortex-pair system as produced from the wing-tip region and the inboard flap. These mechanisms are demonstrated in the results of Fig. 3 based on the analysis given by Crouch.[9] That analysis considered the temporal stability of two vortex pairs, modeled as thin filaments using Biot–Savart integrals. Two vortex pairs are shown after they have propagated downward a distance of about 0.6 vortex spans $\tilde{b}_w$, the distance corresponding to one rotation of the flap vortices about the tip vortices for the conditions $\Gamma_f = 0.33$ and $\delta = 0.3$. The size of the initial perturbation is essentially the same for the three cases, but the wavelengths and phases are different. Figure 3a shows the level of growth and the natural mode shape resulting from the long-wavelength instability. This instability is similar to the Crow instability[5] in that the vorticity centroids are perturbed on each side of the aircraft. However, there is a transient-growth mechanism associated with this long-wavelength instability as shown in Fig. 3b. Transient growth can rapidly amplify perturbations, but this rate of growth is only temporary. The level and duration of the transient growth depends on the parameters Γ_f and δ. Figures 3a and 3b differ only in the phases of the initial perturbations. Figure 3c shows the growth and mode shape resulting from the short-wavelength instability.

These growth mechanisms carry over to the more general system of three trailing-vortex pairs shown in Fig. 1. The three-vortex-pair system involves complex nonperiodic dynamics that inhibit a simple modal analysis of the perturbation growth, thus the initial value problem must be solved numerically. However, as discussed in Sec. II.A, in the typical scenario the tail vortices are destroyed after a short time, and so most of the instability growth occurs on the two-pair system. These new growth mechanisms can be exploited to enhance the vortex destruction with a modest level of forcing imposed by the generating aircraft.

III. Active Control for Flaps-Down Configurations

In operation, the active system uses periodic oscillations of the control surfaces to shift a small amount of lift inboard and outboard

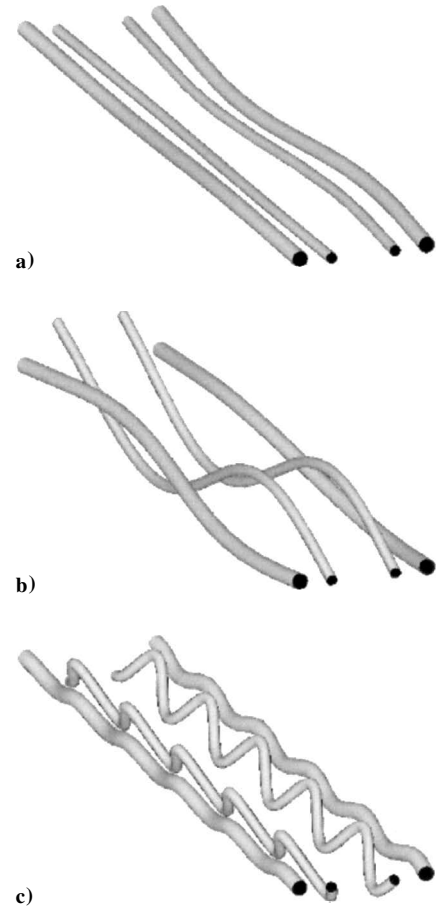

Fig. 3 Growth mechanisms demonstrated for two trailing-vortex pairs; vortex distortions at a fixed time due to a) long-wavelength instability, b) long-wavelength transient growth, and c) short-wavelength instability.

along the wings. The outboard ailerons and the inboard flaperons (and/or spoilers) are driven symmetrically, that is, producing no rolling moment, but 180 deg out of phase, to preserve total airplane lift. Any variation in the pitching moment is trimmed out using the elevator. The form of the forcing function is illustrated by the changes in the spanload over a forcing cycle and the resulting change to the near-field vorticity. The net effect of the oscillations is to introduce spatially periodic perturbations to the wing-tip and inboard-flap vortex positions. When viewed from the ground, these perturbations are wavy distortions along the axes of the vortices.

A. Active-Control Forcing Functions

The active-forcing input can be characterized by a wavelength and by the phases and amplitudes of the tip- and flap-vortex perturbations. The wavelength λ (or wave number $\alpha = 2\pi/\lambda$) of the induced perturbation is selected to produce maximal instability growth. This is set by the frequency of the control-surface oscillation through the relation $\lambda = V_A/f$, where V_A is the aircraft velocity and f is the frequency. The perturbation phases are set by the changes in the wing spanload over the forcing cycle. Figure 4 shows the spanload extremes, the vortex perturbations, and the vorticity-centroid perturbations for the current system and that proposed by Crow and Bate.[4] The vorticity-centroid spacing is given by b. The perturbation amplitude is expressed as a peak-to-peak lift fluctuation $\Delta C_L/C_L$, that is, the amount of lift that is shifted between inboard and outboard stations ΔC_L, normalized by the total wing lift C_L. Note that the control-surface deflection angles will depend on the model geometry but that the lift fluctuation is model independent.

The spanload in Fig. 4a shows a drop corresponding to the inboard flap edge consistent with aircraft in a landing configuration. The current active system shifts a small percentage of lift between inboard and outboard sections of the wing, producing spanwise perturbations to the flap and tip vortices. As the flap vortices are moved

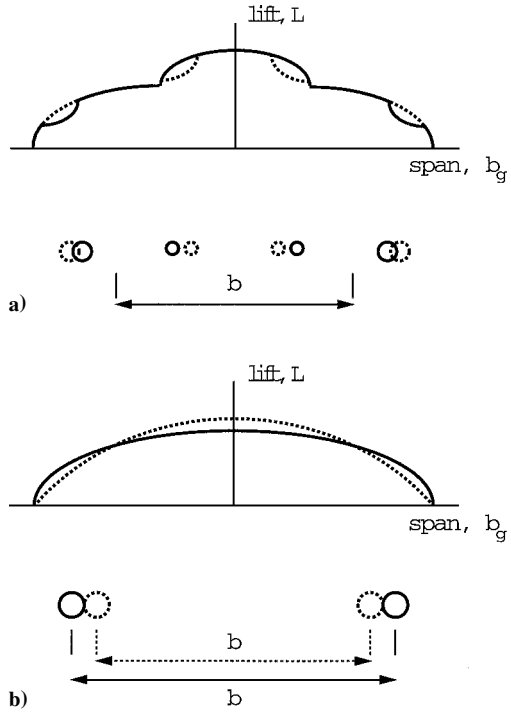

Fig. 4 Spanloads, vortex positions (circles), and vorticity centroids (vertical bars) showing the extremes of active forcing (solid and dashed lines) for a) current system and b) system based on excitation of the Crow instability taken from Crow and Bate.[4]

outboard, the tip vortices are moved inboard, leaving the vorticity centroid of the whole wing essentially unperturbed. Note that the Crow instability,[5] like the long-wavelength instability considered in Sec. II.B, amplifies perturbations to the vorticity centroids. Thus, the forcing function of Fig. 4a does not directly excite the Crow instability.

An excitation of the Crow instability,[5] for example, as considered by Crow and Bate,[4] is achieved through a vorticity-centroid perturbation using the forcing function characterized by Fig. 4b. To keep the lift constant with vorticity-centroid perturbations, the circulation must also change. This, in turn, requires a shift in the wing-root loading, as shown in Fig. 4b.

The form of the spatial perturbation shown in Fig. 4a is chosen to provide an excitation of the new growth mechanisms that more rapidly amplify the perturbations into large distortions of the vortices. When these distortions are large enough, they lead to the breakup of the vortices into vortex rings.

B. Numerical Simulation of Forced Breakup

The current scheme for breaking up the trailing vortices has been studied using numerical simulations. The code is written to solve the incompressible Navier–Stokes equations using Fourier series in all three directions, dealiasing by the two-third rule, with the Corral–Jiménez treatment in the lateral direction y (Ref. 14). This treatment effectively makes the domain infinite in y, rather than periodic (provided the resolved domain is wide enough to prevent any vorticity from reaching its edge). Periodicity in the streamwise direction x is motivated by the rather weak growth of perturbations within one wavelength, $\Delta t = \lambda / V_A$. It amounts to substituting a temporal problem for the exact spatial/temporal problem. Periodicity in the vertical direction z amounts to stacking identical systems of trailing vortices. The straining imposed by these image vortex pairs is an error, which is controlled by setting the vertical box height L_z to sufficiently large values. An infinite domain would be preferable, of course, but the algorithm for that (as in Ref. 12) is more complex and also much less flexible regarding the y and z dimensions of the resolved domain.

The flowfield is made symmetric in the x and y directions so that the computational domain covers a half-wavelength, on one side of the centerline. The whole domain is shown in Fig. 5 for clarity. The initial flowfields are obtained most conveniently by applying a body force over the first very short time step Δt_0. The initial streamwise vorticity ω_x is provided by wake surveys measured in the wind tunnel (similar to Fig. 2, but including control surface deflections), and the interpolation in x uses a cosine function. The time integration is by a low-storage Runge–Kutta/Crank–Nicolson scheme with peak Courant–Friedrichs–Lewy number of 1.7.

Simulations with grids up to 512^3 for the whole domain (10×10^6 independent modes) have been conducted but become too slow to compute using workstations. The simulations begin on coarse grids and automatically stop for regridding when the spectrum drop in any direction becomes insufficient. In each direction, the code compares the kinetic energy associated with the highest wave number currently resolved ($k = k_{\max}$) and the combined kinetic energy associated with the first two wave numbers ($k = 0$ and $2\pi/L$). If the ratio exceeds 10^{-5}, the run produces a warning of which direction is in violation and stops. The maximum wave number in that direction is increased by roughly 40%, the new empty Fourier modes are set to zero, and the simulation is continued. Typically, the energy contained in the upper 30% of the spectrum is 0.01% of the total energy. Because the slope of the spectrum is near −3 as a power law, this gives the estimate of the energy that would have been associated with these empty modes, roughly 0.004%. In that sense, the truncation error is around 0.004% if measured by its energy and 0.6% if measured by its amplitude. Runs with a tighter tolerance than 10^{-5} produced visual differences in the jagged region after pinching but not in the pinching time.

The highest practical circulation Reynolds number Γ_w/ν is about 2×10^4. Comparisons between Reynolds numbers of 10^4 and 2×10^4 are valid sensitivity tests, but, of course, they do not accurately reflect the effect of small-scale turbulence that exists at $\Gamma/\nu = \mathcal{O}(10^7)$.

Figure 5 shows a sequence from the early development of a three-vortex-pair system subjected to an initial perturbation similar to Fig. 4a, with $\Delta C_L/C_L = 6\%$ and wave number $\alpha = 0.8$. The simulations were initialized with wind-tunnel wake-survey data at $\tau = 0.2$, that is, at the same station shown in Fig. 2b. By $\tau = 0.5$, the tail vortices are beginning to cancel on the centerline, and the tip vortices show a peak-to-peak perturbation of $\Delta y_T \approx 0.057$ and $\Delta z_T \approx 0.038$; the centroid of circulation is essentially unperturbed. The perturbations rapidly amplify as the flap vortices orbit the tip vortices. The disturbance growth is consistent with the linear stability theory for two trailing-vortex pairs until $\tau \approx 2.5$ (Ref. 9). This leads to pinching of the dominant tip vortices at $\tau \approx 3.1$.

To compare the amplification rate to the instability of Crow,[5] we introduce the timescale τ_0 based on the total half-plane circulation Γ_0 and its centroid separation b_0, $\tau_0 = \tau(\Gamma_0/b_0^2)$. In general, the total circulation can vary with time due to cancellation on the centerline so that the values Γ_0 and b_0 are taken from the initial survey. For the simulation initiated at $\tau = 0.2$, $\tau_0 = 0.74\tau$. The tip-vortex perturbation $[\Delta y_T^2 + \Delta z_T^2]^{1/2}$ amplifies by the ratio 0.94/0.068 over the period $\Delta\tau_0 = 0.74(2.5 - 0.5)$ yielding an effective growth rate of 1.8, more than twice the value for the Crow instability. Note that in the absence of the flap vortices, tip perturbations would amplify on a timescale $\tau_T = \tau(\Gamma_T/b_T^2) \approx 0.6\tau$. In terms of this tip-vortex timescale, the effective amplification rate is 2.2.

Numerical simulations initiated with wind-tunnel data at $\tau = 0$, that is, the survey location of Fig. 2a, can differ significantly from simulations initiated at $\tau = 0.2$, that is, the survey location of Fig. 2b. This is due to the tail vortices, which persist longer in the simulations initiated at $\tau = 0$. The tail vortices primarily affect the flap-vortex perturbations, with only a weak effect on the tip vortices. Nonetheless, the effects on the pinch time can be large. Simulations initiated with surveys at $\tau = 0$ also show a greater sensitivity to Reynolds number. For all of these reasons, simulations from $\tau = 0$ have proven less useful. This is attributed to the lack of small-scale turbulence and the shear in the body wake.

IV. Towing-Tank Validation Experiments

To validate the basic concept of vortex breakup, exploiting the new growth mechanisms, a series of ground-based tests were conducted. The breakup of the vortices was expected to occur at

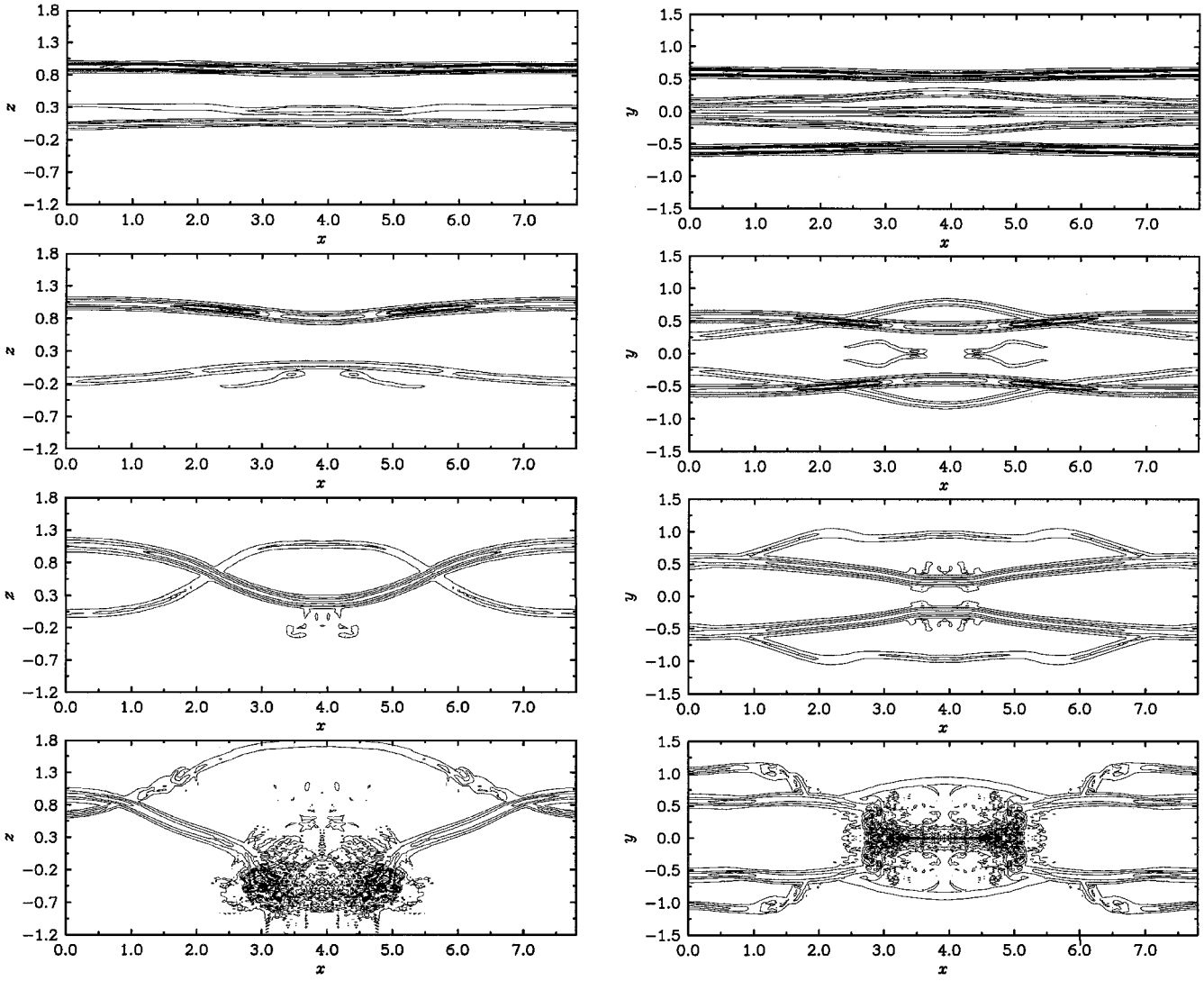

Fig. 5 Side view (left) and top view (right) of vortices from numerical simulations for conditions of Fig. 2: $\tau =$ 0.5, 1.5, 2.5, and 3.5 (top to bottom); contours of vorticity magnitude.

distances greater than 50 spans downstream of the generating aircraft. Because this is well beyond the distances achievable in good flow-quality wind tunnels with sufficient model size, the demonstration test was conducted in a water towing tank. The design of the towing-tank model made use of wind-tunnel experiments to ensure that it captured the essential features of real commercial aircraft and to ensure that it worked well at the test Reynolds numbers. The horizontal tail span and the diameter of the circular cross-sectional body were scaled to typical commercial transport airplanes.

The approach for concept validation involves three basic steps. First, the near-field vorticity is measured behind commercial aircraft in the flaps-down approach configuration. This is done in a wind tunnel using conventional high-lift models by means of the five-hole probe wake survey technique of Crowder et al.[13] Second, the near-field vorticity is measured behind the towing-tank test model, using the same technique. These results are used to determine how well the towing-tank model represents the conventional-model vorticity field. Finally, the model is tested in the towing tank to study the far-field evolution of the vortices. This is done with the model passive and with active control.

A. Test Description

Experiments on the active breakup of trailing vortices were conducted in the U.S. Navy David Taylor Model Basin shallow water basin. The towing tank is more than 350 m long, 15.5 m wide, and 6.7 m deep. The wing of the test model has a 0.91-m span. For the results presented here, the model was positioned 1.8 m below the water surface, and the carriage speed was 4 m/s. This resulted in a chord Reynolds number of 6×10^5, and a vortex Reynolds number of $\Gamma_w/\nu = 5 \times 10^5$. The wind-tunnel tests used to measure the initial vorticity fields were conducted at the same Reynolds numbers.

The model scale was chosen to permit the vortices to descend for more than four geometric spans before entering ground effect and also to avoid end effects due to perturbations generated during the acceleration and deceleration of the model. Perturbations to the wake were achieved by moving the inboard and outboard ailerons in prescribed motion, as described earlier. Towing velocity and lift forces were measured to provide a time history of C_L with 0.3% accuracy. Forcing amplitudes were known to within 8% of their nominal value and were measured by calibration of $\Delta C_L/C_L$ using separate runs in which only one aileron pair (inboard or outboard) were in motion. The objective of maintaining constant lift while perturbing the wake was typically met to within 0.5% of total lift.

The model has an unswept wing without taper to accommodate a torque-tube linkage that moves inboard and outboard ailerons. The airfoil, designed for the test Reynolds number, consists of a basic section having constant chord and a thin, cambered, trailing-edge section with a chord that can be varied between 0 and 67% of the basic airfoil chord. Simple sheet metal working techniques are employed to create these trailing-edge sections, and an assortment of them were produced to simulate the highly loaded, partial span flaps and more lightly loaded ailerons of various airplane configurations. Wakes similar to those of a variety of different airplanes are simulated in this manner. Vorticity distributions from wind-tunnel wake survey measurements at 1–4 wing spans downstream of the towing tank model and several airplane models compare favorably.

The trailing vortices were visualized using fluorescent dye injected at the outer edge of the inner flap, the outer edge of the outer flap, the wing tip, and the horizontal tail. When necessary, dye could also be injected into the side of body vortices. A 12-m section of the towing tank was illuminated using 14 swimming-pool lights. Time-coded video cameras were placed at various positions to monitor the evolution of the vortices. A laser light sheet at the upstream end of the lit section provided a cross section, that is, end view, of the vortices.

B. Vortex Breakup

To evaluate the basic concept of the active system, a range of parameters have been considered rather than any specific airplane configuration. This parameter range was selected to be representative of existing commercial aircraft. The wing parameters (measured at the tail plane) covered the range $0.25 \leq \Gamma_f \leq 0.35$ and $0.35 \leq \delta \leq 0.45$. Three different tail spans, and many different tail angles, were considered. The range of tail settings account for different configurations as well as differences in the airplane center of gravity. The forcing functions used in the towing-tank test are determined from wind-tunnel wake surveys similar to Fig. 2. These surveys show the initial vorticity fields behind the model. In addition to the baseline conditions, the vortex positions were measured at the peaks of the forcing, with control surfaces in their deflected positions.

The primary metric used to evaluate the system performance is the vortex pinch time, that is, the time required for the vortices to link into vortex rings. This was based on flow visualizations and measured from the video recordings. Quoted pinch times have an error of less than 0.1τ. Figure 6 shows the side view of the vortices (without active forcing) at the dimensionless time intervals: $\tau = 0.5$, 1.5, 2.5, and 3.5. These results are for the same parameters as given in Figs. 2 and 5. In the absence of forcing, the vortices show very little waviness. In fact, the vortices propagate to the floor and separate due to ground effects without pinching.

In this sequence of flow visualization, and in those that follow, the tip vortex that is, outboard flap vortex plus wing tip vortex, is marked distinctly and persists as a concentrated column of dye. The inboard flap and tail vortices constitute the more diffusely marked region that originates beneath the tip vortex and then spreads. The diffuse image of the flap vortex implies spreading of the vorticity comprising it, but the present results do not allow this to be quantified. In simulations, for example, Fig. 5, vorticity contours describing the flap vortex are not as diffuse as the experimental dye visualization implies. Perhaps the lower Reynolds number of simulations is responsible for the difference (if turbulence is suppressed), but the otherwise good agreement between simulation and experiment suggests that flap vortices either are not as diffuse as they appear to be or that their being diffuse does not significantly change the evolution of the vortex system. The simulations are devoid of any axial flow or short-scale perturbations in the initial conditions.

For general comparison to flight conditions, it is useful to introduce the timescale $\tau_{\text{ell}} \equiv \tau(\Gamma_{\text{ell}}/b_{\text{ell}}^2)$, based on an elliptic spanload approximation for the same airplane lift. The vortices in the absence of forcing persist beyond $\tau_{\text{ell}} \approx 5.4$. This translates to a distance of approximately 6.5 n mile behind a 747-400 flying at 150 kn. The long persistence of the vortices is consistent with quiet atmospheric conditions; atmospheric turbulence is known to accelerate the destruction of the vortices. Thus, the towing-tank simulated a worst-case condition for a following aircraft.

Figure 7 shows the side view of the vortices for the same conditions of Fig. 6, except now with active forcing. The peak-to-peak forcing level is $\Delta C_L/C_L = 6\%$ and the wave number $\alpha = 0.8$. Time intervals in this sequence match those in Fig. 6. The sequence in Fig. 7 shows the growth of waviness on the tip vortex that ultimately leads to vortex reconnection on the y centerline. One streamwise wavelength is captured here, but the waveform is periodic in the streamwise x direction and matches the imposed wavelength of forcing. For this case, pinching occurs at $\tau = 3.3$ (or $\tau_{\text{ell}} \approx 2$).

The experimental results are in good agreement with the numerical simulations presented in Fig. 5. When the total circulation at $\tau = 0.2$ (i.e., from the survey station of Fig. 2b) is used for the nondimensionalization, the pinch time is $\tau_0 = 2.4$. For the same

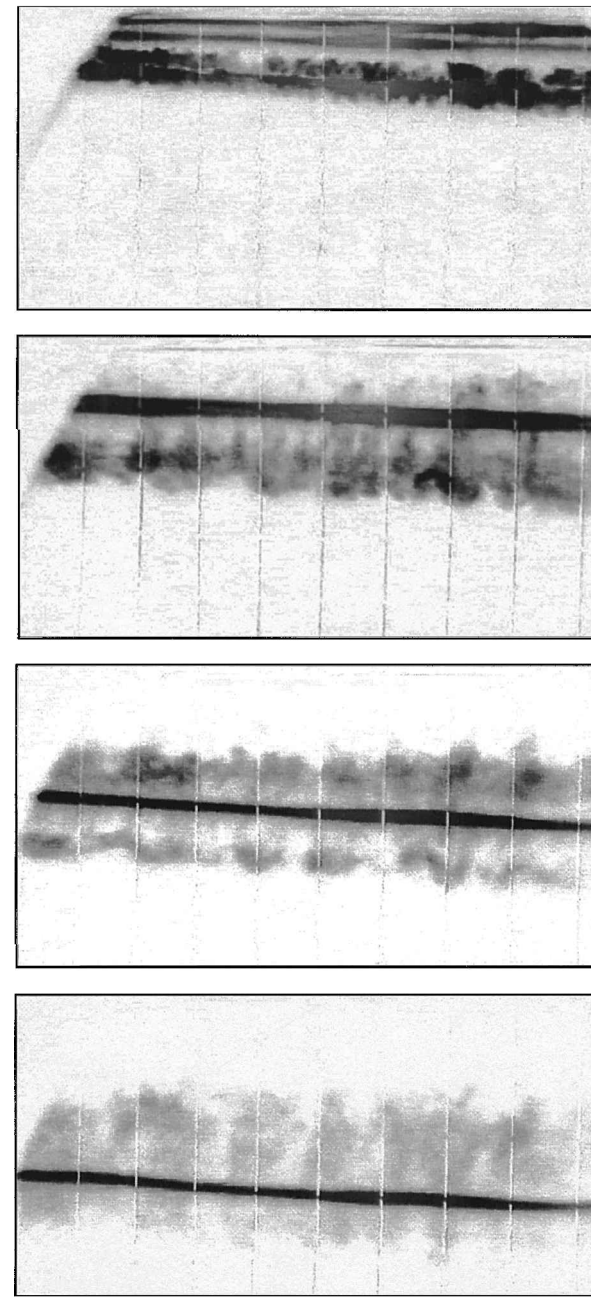

Fig. 6 Side views of trailing vortices unforced for conditions of Fig. 2: $\Gamma_f = 0.26$; $\delta = 0.42$; $\Gamma_t = -0.22$; and $\tau =$ 0.5, 1.5, 2.5, and 3.5 (top to bottom).

definition of τ_0, the numerical simulation results showed pinching at $\tau_0 \approx 2.3$. In terms of the elliptic spanload scaling, the pinch time is $\tau_{\text{ell}} \approx 1.8$, which corresponds to approximately 2.5 n mile behind a 747-400. This is a very favorable value considering that the unperturbed vortices persisted beyond 6.5 n mile.

Figure 8 shows the top view of the vortices for a sequence similar to that of Fig. 7. These results are for the same wing configuration as Fig. 7 but with a different tail angle ($\Gamma_t = -0.19$, $y_t = 0.19$, and $z_t - z_w = 0.04$). Two wavelengths are captured here, showing the growth of waviness and vortex reconnection on the centerline. The time intervals begin at $\tau = 1.0$ and increase in steps of 0.5 to $\tau = 4.0$. The greater tail span and weaker tail vortex strength has slowed the evolution from the conditions for Fig. 7, delaying the reconnection event from $\tau = 3.3$ until $\tau = 4.0$.

C. Control Effectiveness

The best results observed in the experiments, for an amplitude of $\Delta C_L/C_L = 6\%$, show vortex pinching at $\tau \approx 3.5$ ($\tau_{\text{ell}} \approx 2$). However, the pinch time (or time to linking) depends on the basic

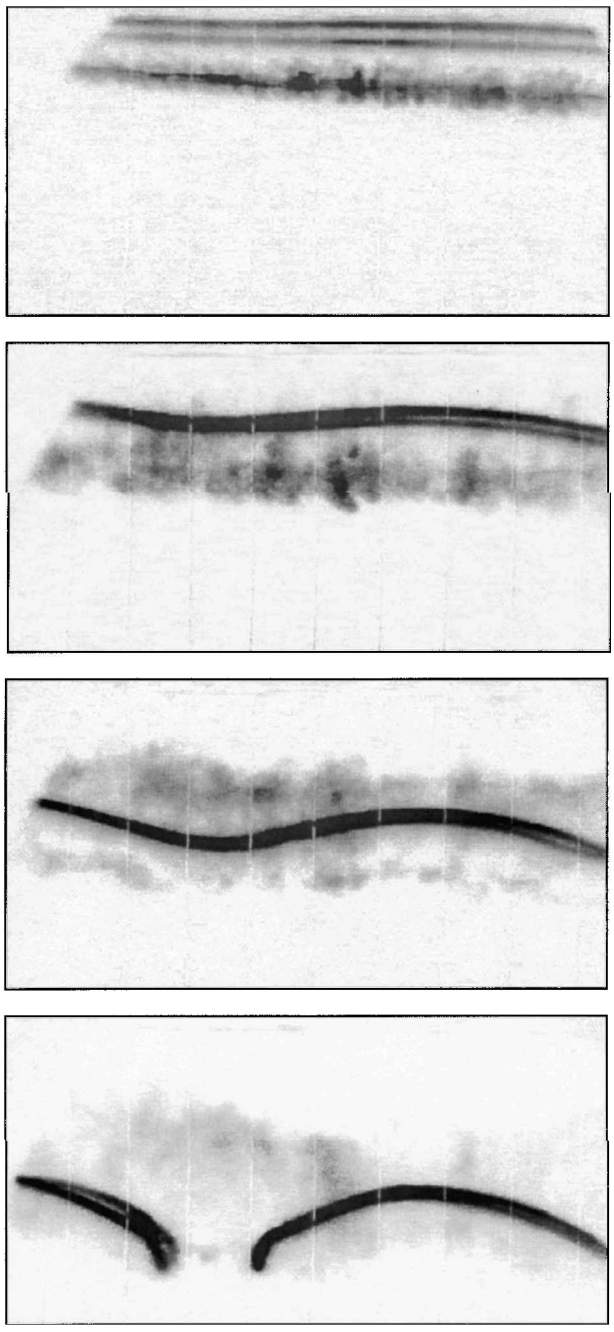

Fig. 7 Side views of trailing vortices with 6% active forcing for conditions of Fig. 2: $\Gamma_f = 0.26$; $\delta = 0.42$; $\Gamma_t = -0.22$; and $\tau = 0.5, 1.5, 2.5$, and 3.5 (top to bottom).

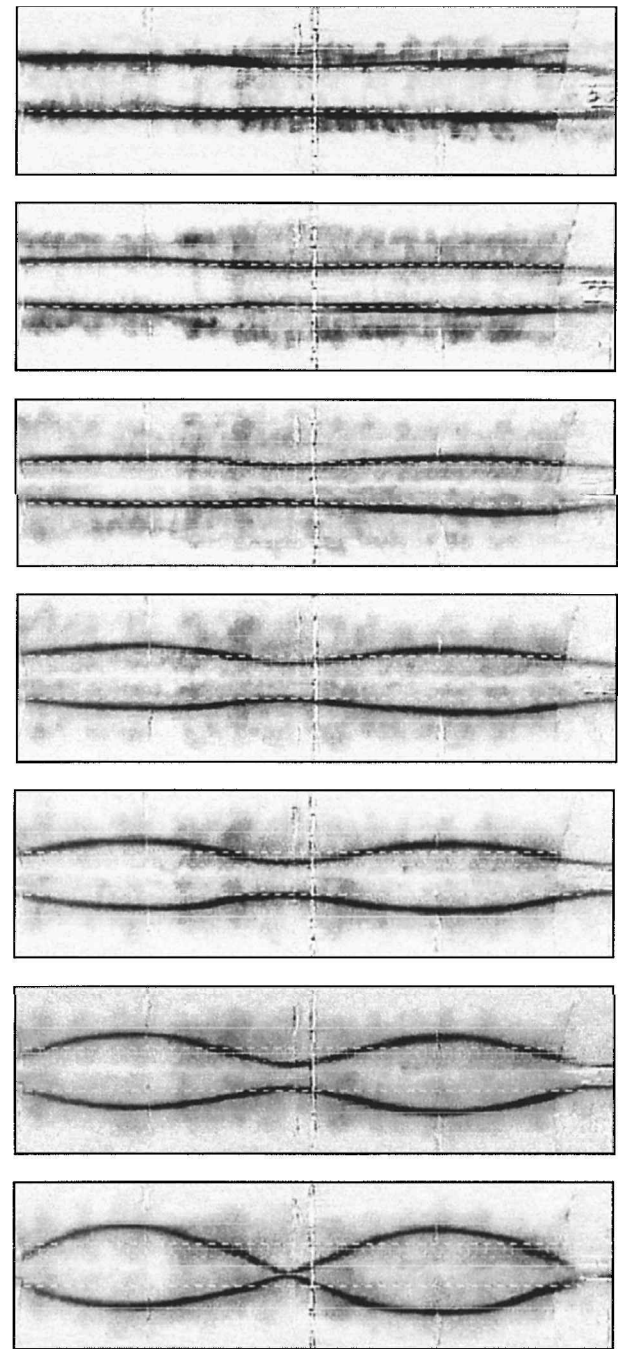

Fig. 8 Top views of trailing vortices with 6% active forcing for the following conditions: $\Gamma_f = 0.26$; $\delta = 0.42$; $\Gamma_t = -0.19$; and $\tau = 1.0, 1.5, 2.0, 2.5, 3.0, 3.5$, and 4.0 (top to bottom).

configuration parameters. Additional time (or distance) may, furthermore, be required after linking before the vortices become benign to a following aircraft. Nonetheless, the time to linking provides a measure of the effectiveness of the active system in breaking up the vortices.

Over the parameter ranges considered ($0.25 \le \Gamma_f \le 0.35$, $0.35 \le \delta \le 0.45$, and $-0.24 \le \Gamma_t \le 0$), the tail-vortex strength Γ_t had the strongest influence on the pinch time, as shown in Fig. 9. The data in Fig. 9 are for a single wing condition ($\Gamma_f = 0.26$ and $\delta = 0.42$), but they include two tail lengths and many tail angles. For tail vortices stronger than 18% of the wing circulation, pinching occurs at $\tau_{ell} \approx 2$. For tail vortices weaker than about 13%, pinching occurs at $\tau_{ell} > 4$. A pinch time of $\tau_{ell} = 2.5$ translates to approximately 3 n mile behind a 747-400 in flight. As an example of the current FAA wake-turbulence separations, a 737 following a 747 must be separated by 5 n mile.

Figure 9 shows that the active system is less effective for weaker tail-vortex circulations. The critical value for the tail strength

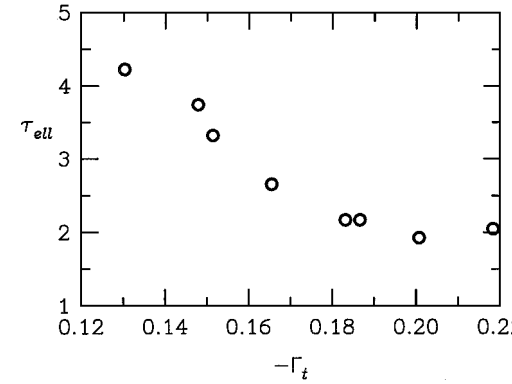

Fig. 9 Nondimensional pinch times as a function of nondimensional tail-vortex strength ($\Gamma_f = 0.26$ and $\delta = 0.42$).

depends on the wing parameters (Γ_f and δ) and the level of forcing $\Delta C_L/C_L$. The tail-vortex strength depends on the airplane configuration (i.e., flaps-down pitching moment, tail moment arm, and tail span) and the airplane center of gravity. Thus, Fig. 9 provides a basis for judging the performance of the active system for a given aircraft.

To further assess the performance of the active system, the towing-tank experiments also examined the forcing of the Crow instability.[5] Because of the control surfaces used for the forcing, the active model is not capable of forcing the Crow instability while holding the total lift constant. The forcing of the Crow instability is achieved by cycling the inboard and outboard control surfaces in phase. Thus, a 6% forcing of the Crow instability resulted in a 6% variation in the lift. The pinch time for a 6% forcing of the Crow instability was $\tau_0 \approx 4.5$ ($\tau_{\text{ell}} \approx 3.3$). When the forcing level was doubled, the pinch time was reduced, consistent with the timescale τ_0 and a growth rate of 0.8 [$\Delta\tau_0 \approx \ln(1/2)/0.8$].

The towing-tank results showed that pinching due to Crow instability[5] forcing also depends on the strength of the tail vortices. As the tail vortices become weaker, the time to pinching is increased. This is counter to expectations based on the findings of Crow and Bate[4] and Bilanin and Widnall[6] (because the total circulation has increased), and it suggests that transient growth may also be significant when exciting the Crow instability[5] for this particular model.

V. Conclusions

Active control can be used to excite multiple-vortex instabilities for the breakup of trailing vortices behind aircraft in the flaps-down configuration. Airplane control surfaces are used to introduce a specific form of perturbation that rapidly amplifies due to the existence of multiple-vortex pairs. The concept has been demonstrated using numerical simulations and validated in towing-tank experiments. Wind-tunnel wake surveys are used as initial vorticity fields for the numerical simulations. The breakup of the vortices in the simulations is in good agreement with the experiments when the simulations are initiated with surveys measured at the downstream location $\tau = 0.2$, which is at about four geometric wing spans. The perturbation growth in the numerical simulations is also in general agreement with the linear stability theory.

Linking times (the time required for the vortices to pinch on the centerline) were measured over a range of parameters representing the key features of commercial aircraft. However, no specific airplane configurations were considered. The effectiveness of the system, in terms of the amplitude required to achieve linking within a given distance, depended on the wing spanload and the horizontal-tail load. The towing-tank results show that early linking can be achieved using an acceptable level of forcing for realistic configurations.

Although the active-system concept has been demonstrated, there are open issues that need to be resolved before the system can be considered for implementation. The most obvious issues fall into one of three groups: issues related to performance in flight, issues related to viability for the active airplane, and issues related to the effectiveness for the following airplane.

Continued analysis and ground-based testing can help assess the potential for application to specific aircraft. However, there are additional unknowns related to differences in the wakes behind aircraft in flight and aircraft models tested on the ground. The most significant of these unknowns is the potential effect of thrust on the near-field evolution of the multiple-vortex system. Most of these issues will be resolved only through a flight test of the concept.

The towing-tank results provide important information for assessing the viability of implementing the system on a given aircraft. The tests provide the level of forcing required to achieve a breakup within a given distance behind the aircraft. When the forcing level is known, control surface deflections can be estimated for specific aircraft in flight. The control surface information can be used to estimate the dynamic loads and the potential impact on ride quality. Pinch time results for the different tail-vortex strengths can be used to determine any limits on the airplane center of gravity. Preliminary estimates of dynamic loads and ride quality impact show the concept to be viable in terms of the active airplane.

Finally, there are practical issues related to the system effectiveness for the following aircraft. This will require a measure of goodness to help determine at what stage in the breakup do the vortices become benign. This will also include environmental effects and ground effects. For example, wind shear could weaken one of the vortices and, thus, influence the growth of perturbations. Ground effects could slow the perturbation growth and delay the breakup or enhance the breakup through viscous effects or turbulent mixing. Atmospheric turbulence is expected to play a favorable role in accelerating the breakup, similar to the unforced condition. Existing flight data and future ground-based testing could help resolve some of these issues before concept flight testing.

Acknowledgments

We are grateful to Wen-Huei Jou for his insightful comments, encouragement, and support from the very early stages of this work. We also want to thank Tanja Krutckoff and Byram Bays-Muchmore for their contributions to the experimental program. Finally, we acknowledge the wonderful support provided by the researchers at the U.S. Navy David Taylor Model Basin, including Thomas Huang, Doug Griggs, and the late John Gordon and Steve McGuigan.

References

[1]Robinson, J. J., "A Simulation-Based Study of the Impact of Aircraft Wake Turbulence Weight Categories on Airport Capacity," CP-584, AGARD, 1996, pp. 22-1–22-15.

[2]Rossow, V. J., "Lift-Generated Vortex Wakes of Subsonic Transport Aircraft," *Progress in Aerospace Sciences*, Vol. 35, 1999, pp. 507–660.

[3]Crow, S. C., *Aircraft Wake Turbulence and Its Detection*, edited by J. Olsen, A. Goldburg, and M. Rogers, 1971, Plenum, New York, pp. 551–582.

[4]Crow, S. C., and Bate, E. R., "Lifespan of Trailing Vortices in a Turbulent Atmosphere," *Journal of Aircraft*, Vol. 13, No. 7, 1976, pp. 476–482.

[5]Crow, S. C., "Stability Theory for a Pair of Trailing Vortices," *AIAA Journal*, Vol. 8, No. 12, 1970, pp. 2172–2179.

[6]Bilanin, A. J., and Widnall, S. E., "Aircraft Wake Dissipation by Sinusoidal Instability and Vortex Breakdown," AIAA Paper 73-107, 1973.

[7]de Bruin, A. C., Hegen, S. H., Rohne, P. B., and Spalart, P. R., "Flow Field Survey in the Trailing Vortex System Behind a Civil Aircraft Model at High Lift," CP-584, AGARD, 1996, pp. 25-1–25-12.

[8]Crouch, J. D., "Stability of Multiple Trailing-Vortex Pairs," CP-584, AGARD, 1996, pp. 17-1–17-8.

[9]Crouch, J. D., "Instability and Transient Growth for Two Trailing-Vortex Pairs," *Journal of Fluid Mechanics*, Vol. 350, 1997, pp. 311–330.

[10]Rossow, V. J., "Wake Hazard Alleviation Associated with Roll Oscillations of Wake-Generating Aircraft," *Journal of Aircraft*, Vol. 23, No. 6, 1986, pp. 484–491.

[11]Barber, M. R., and Tymczyszyn, J. J., "Wake Vortex Attenuation Flight Tests: A Status Report," NASA CP-2170, 1980, pp. 387–408.

[12]Rennich, S. C., and Lele, S. K., "Method for Accelerating the Destruction of Aircraft Wake Vortices," AIAA Paper 98-0667, 1998.

[13]Crowder, J. P., Watzlavick, R. L., and Krutckoff, T. K., "Airplane Flow-Field Measurements," World Aviation Congress Paper 975535, 1997.

[14]Corral, R., and Jiménez, J., "Fourier/Chebyshev Methods for the Incompressible Navier–Stokes Equations in Infinite Domains," *Journal of Computational Physics*, Vol. 121, 1995, pp. 261–270.

J. C. Hermanson
Associate Editor